Fluoro-2,6-dimethylphenyl mono-hydroxychlorin and porphyrin congeners

Cierra Brown, Brandon M. Campbell, Tina Chen, Richard K. Darkwa, Geena Kim, Danielle J. Kranchalk, Hannah Lamport, Colin M-D. Le, Jenny Lu, Giovan N. McKnight, Nejc Nagelj, Nikhil V. Seshadri, Kristopher G. Reynolds, Shao-Liang Zheng and Dilek K. Dogutan*

Department of Chemistry and Chemical Biology, Harvard University, 12 Oxford Street, Cambridge, MA 02138, USA

Received date (to be automatically inserted after your manuscript is submitted)
Accepted date (to be automatically inserted after your manuscript is accepted)

ABSTRACT: Mono-hydroxychlorins are uncommon macrocycles that have only been synthetically realized by modifying porphyrin rings using the harsh oxidizing agent OsO_4. We show here that a more directed delivery of the mono-hydroxychlorin may be concomitantly obtained from oxidation of porphyrinogen using the mild conditions of the high dilution Lindsey porphyrin forming reaction where water content is minimized by using dry $CHCl_3$ within the environment of a glovebox. We now report the direct synthesis of 17,18-dihydro-18-hydroxy-5,10,15,20-*tetrakis*-(4-fluoro,2,6-dimethylphenyl)-porphyrin (**2H-TFChl-$^{\beta}$OH**) together with the corresponding freebase porphyrin **TFP**. The **TFP** has been metalated with $FeBr_2$ and $MgBr_2{\cdot}OEt_2$ resulting in metalloporphyrins **Fe(III)TFP(Cl)** and **Mg(II)TFP** which have been structurally characterized by single-crystal X-ray crystallography. We find that the excited state properties of the mono-hydroxychlorin are similar to that of its parent **TFP** and **Mg(II)TFP** porphyrin congeners. Excited state deactivation by vibronic coupling to the high energy O–H oscillator is circumvented with the hydroxyl group remote to the 18π-electron framework of the chlorin ring. These results reveal that strong H-bonding groups may be introduced on the periphery of chlorin ring while maintaining the light gathering properties that lie at the heart of photosynthesis of the chlorin ring.

KEYWORDS: Porphyrin, chlorin, mono-hydroxychlorin, magnesium porphyrin, iron porphyrin, metalation, crystal structure, emission, and absorption spectroscopies.

*Correspondence to: Dilek K. Dogutan, email: dkiper@fas.harvard.edu, +1 617 495 3297.

INTRODUCTION

Chlorins are aromatic macrocycles bearing a conjugated 18π-electron pathway. Owing to their fundamental importance as the macrocyclic core of chlorophylls, chlorins have been the targets of a wide range of synthetic methods.[1] Whereas the earliest synthesis of chlorins was as a byproduct of porphyrin synthesis, a more directed delivery of the chlorin can be achieved from porphyrinogen, which is the 6 e^-, 6 H^+ reduced tetrapyrrolic precursor of porphyrin.[1,2] Numerous chlorins have been obtained with a bewildering array of peripheral substituents. Substitution of dihydroxy groups at the *β,β′*-position of the reduced pyrrole of the chlorin ring is provided by initial oxidation of the pyrrole with OsO_4.[3–7,9] However, there are few chlorins featuring a mono-hydroxylation at the *β*-position of the reduced pyrrole of the chlorin framework because synthetic methodologies leading to mono-hydroxychlorins are significantly underdeveloped. Indeed, there are only two reports affording mono-hydroxychlorins, both of which require the use of OsO_4 to hydroxylate the *β,β′*-position of the pyrrole.[10,11] We sought to place a hydroxyl group at the reduced *β,β′*-pyrrolic double bond of the chlorin more directly under mild conditions while avoiding the use of OsO_4, as new methods are continually being sought to replace this toxic and corrosive reagent.[12,13] The mono-hydroxychlorin might be obtained by modifying the conditions under which the porphyrinogen is generated during porphyrin synthesis. In pursuing these studies, we have found 4-fluoro-2,6-dimethylphenyl substituents on pyrrole macrocyclic platforms to be a useful synthon with regard to both synthetic versatility and the utility of the fluoro group as a handle for NMR characterization.[14] Taking advantage of the modified high dilution statistical porphyrin forming reaction,[15] we now report the direct synthesis of 17,18-dihydro-18-hydroxy-5,10,15,20-*tetrakis*-(4-fluoro,2,6-dimethylphenyl)porphyrin (**2H-TFChl-$^{\beta}$OH**) under mild conditions together with the corresponding freebase porphyrin **TFP**. The **TFP** has been further metalated with $FeBr_2$ and $MgBr_2{\cdot}OEt_2$, which have been structurally characterized by single-crystal X-ray crystallography.

The presence of a hydroxyl group is an important stabilizing element in biology.[16–18] However, the hydroxyl group on the chlorin macrocycle can, in principle, perturb its excited state properties. The high energy O–H oscillator often provides a facile nonradiative pathway for excited state decay through vibronic coupling[19,20] or through proton transfer arising from photoacidity.[21] In this regard, time-resolved spectroscopic studies of the excited state of the porphyrins and *monohydroxy* chlorin are illuminating. To rigorously examine the perturbation of hydroxyl group on the excited state properties of the chlorin ring, we sought to provide a side-by-side comparison of mono-hydroxychlorin and porphyrin analogs. Whereas the excited state properties of the 18π-electron circuit of the porphyrin is circumvented by the low lying d-d ligand-field states of the **Fe(III)TFP(Cl)** center, as is well established in heme chemistry, the **Mg(II)TFP** complex like **TFP**, exhibits strong fluorescence and appreciable excited state lifetimes of chlorophylls.[22] Interestingly, this fluorescence is preserved in **2H-TFChl-$^{\beta}$OH**, and indeed the lifetime of the chlorin is on par with its porphyrin **TFP** and **Mg(II)TFP** congeners. With the hydrogen bonding remote O–H group to the 18π-electron framework of the chlorin ring, the excited state properties of the chlorin ring are preserved. These results reveal that strong H-bonding groups may be introduced to a chlorin ring while maintaining the light gathering properties that lie at the heart of photosynthesis of the chlorin ring.

RESULTS AND DISCUSSION

Synthesis and Characterization of Mono-Hydroxychlorin and Metalated TFP Porphyrins. The freebase porphyrin (**TFP)** and mono-hydroxychlorin (**2H-TFChl-$^{\beta}$OH)** were prepared by the route shown in Figure 1. The use of modified high-dilution Lindsey porphyrin forming reaction delivers TFP in appreciable isolated yield when $CHCl_3$ containing 0.5–1% EtOH as a stabilizer was (1) first distilled over K_2CO_3, (2) degassed with three consecutive freeze-pump-thaw cycles, and (3) dried over activated molecular sieves (3 Å) to remove any remaining trace amounts of water. The control experiments lacking steps 1-3 afforded either no porphyrin or very poor isolated yields (~1%) likely due to water quenching BF_3•OEt_2 leading to reduce the formation of the corresponding porphyrinogen. In addition to the porphyrin, we have made the finding that mono-hydroxychlorin may be obtained concomitantly during the chemical oxidation of the porphyrinogen intermediate in a nitrogen filled glovebox in dark. Although four consecutive electrophilic aromatic substitution reactions result in the formation of four molecules of water for every molecule of porphyrinogen formed, drying $CHCl_3$ prior to the porphyrinogen forming reaction (see Experimental) and performing the condensation reaction giving the porphyrinogen in a nitrogen-filled glovebox significantly *improved* the overall isolated yield of **TFP** (12–15% vs 3%) and also afforded **2H-TFChl-$^{\beta}$OH** (3%) at an isolated yield that is comparable with the previously reported mono-hydroxychlorins.[10,11] The key advantage of this modified synthesis is the ability to access to mono-hydroxychlorin at room temperature and under mild conditions without the need to use the corrosive and toxic OsO_4 reagent.

The mono-hydroxychlorin **2H-TFChl-$^{\beta}$OH** has been thoroughly characterized by ^{1}H NMR (Figs. S1–S6), ^{13}C NMR (Fig. S7), ^{19}F NMR (Fig. S8), ^{1}H-^{1}H COSY (Figs. S9–S14), IR spectroscopy (Fig. S15) and high-resolution mass spectroscopy (Fig. S16). The NMR spectra of **2H-TFChl-$^{\beta}$OH** are informative. The chemical shifts of protons at the 17 and 18 positions of the macrocycle (3.81 ppm and 4.10 ppm (two diastereomeric protons) and 6.06 ppm, respectively) and the 18-hydroxyl group (2.26 ppm J = 4 Hz) resonances and chemical shifts are similar to those reported for the previously prepared *mono*-hydroxychlorins.[10,11] ^{1}H–^{1}H COSY NMR spectrum (Figure S11) clearly shows the spin-spin couplings between the protons at the 17 and 18 positions. The most apparent cross-peaks on the spectrum are observed between protons at the 17 and 18 positions at 4.10 ppm and 3.81 ppm. As expected between the two diastereomeric protons at the 17 position, the *cis*-coupling constant is smaller than the *trans*-coupling constant. ^{1}H-^{1}H COSY NMR spectrum provides further verification that the proton at the 18 position is also coupling with the hydroxyl proton resulting in the well defined doublet on the ^{1}H NMR spectrum at 2.26 ppm (Figure S5). Additionally, on the ^{1}H NMR spectra, the 8 distinct *β*-pyrrolic CH protons are observed between 8.08 ppm and 8.41 ppm and the 8 phenyl protons are obtained as a multiplet between 7.09 ppm and 7.22 ppm (Figure S2). The proton on the 18 position is also observed as a multiplet at 6.06 ppm due to coupling to the diastereomeric protons at the 17 position as well as coupling to the hydroxyl proton on the 18 position (Figs. S3 and S4). The diastereomeric protons at the 17 position appear as two doublets of doublets at 3.81 ppm and 4.10 ppm with a *cis*-coupling constant of 1.6 Hz and a *trans*-coupling constant of 7.6 Hz, respectively, consistent with the pyrrolidine ring geometry (Figs. S3 and S4). In addition, the geminal proton coupling constant is observed to be 18.0 Hz (Fig.

S3). The 8 proton signals between 1.73 ppm and 2.06 ppm with the integration of 3 protons each are due to the 8 distinct CH_3 groups (Fig. S5) and are confirmed to be singlets using the ^{1}H-^{1}H COSY spectrum (Fig. S13). The 8 distinct methyl resonances confirm the low C1 symmetry of **2H-TFChl-$^{\beta}$OH**. There is only one peak observed below 0 ppm, appearing at –1.69 ppm, due to the two inside NH protons (Fig. S6). The ^{1}H-^{1}H COSY spectrum confirms the absence of coupling of the inside NH protons to any other protons (Fig. S14), which is convincing evidence for non-contamination by another macrocycle such as **TFP**. The proton decoupled ^{19}F NMR spectrum shows (Fig. S8) 4 distinct peaks which is consistent with the four fluorines situated in four different chemical environments due to broken symmetry (C1) of **2H-TFChl-$^{\beta}$OH**.

Metalation of **TFP** using $FeBr_2$ and $MgBr_2{\cdot}OEt_2$ were proceeded by deprotonation of the internal N–H pyrrolic protons in the presence of 2,4,6-trimethylpyridine or triethylamine to obtain **Fe(III)TFP(Cl)** and **Mg(II)TFP**, respectively. Completion of the metalation reactions was confirmed with TLC analyses. Magnesium insertion was monitored with neutral alumina plates as magnesium complexes are known to be acid labile[23] and undergo demetallation on slightly acidic silica TLC plates. An aqueous workup was followed with a short silica column filtration affording **Fe(III)TFP(Cl)** in 40.4% isolated yield; purification of **Mg(II)TFP** with a short neutral alumina patch afforded the compound in 80% isolated yield. The full characterization of **Mg(II)TFP** was conducted with ^{1}H NMR (Figs. S17 and S18), ^{19}F NMR (Figs. S19), ^{13}C NMR (Fig. S20), IR spectroscopy (Fig. S21), and high-resolution mass spectrometry (Fig. S22). **Mg(II)TFP** ^{1}H NMR spectrum confirms disappearance of the inside pyrrolic NH resonances and ^{13}C NMR spectrum shows the typical resonances for fully symmetric metalated A4 porphyrin. In the ^{19}F NMR spectrum, the triplet at –117.16 ppm arises from coupling the two chemically equivalent protons located on the 3 and 5 positions of the 4-fluoro,2,6-dimethylphenyl group. Due to the paramagnetic nature of the **Fe(III)TFP(Cl)**, ^{1}H NMR spectra were uninformative (Fig. S24) but the ^{19}F NMR spectrum of revealed a singlet at –113.89 ppm due to the tetragonal symmetry nature of the iron porphyrin (Fig. S25). To further investigate the oxidation state of the iron center, zero-field ^{57}Fe Mössbauer spectrum was measured (Figure 2A). The delta isomer shift for **Fe(III)TFP(Cl)** is 0.35 mm/s and a quadruple splitting of 0.77 mm/s , consistent with an Fe(III) oxidation state.[24] The g = 6 and g = 4 signals in the EPR spectrum of **Fe(III)TFP(Cl)** (Figure 2B) are in accordance with the g-values of high spin Fe(III) porphyrins.[25] Thus, the EPR spectroscopy supports the presence of a high spin Fe(III) d^5 system (S = 5/2). Further characterization of **Mg(II)TFP** and **Fe(III)TFP(Cl)** was provided by single-crystal X-ray diffraction (Figure 3).

Mg(II)TFP crystallized in the $P\bar{1}$ space group with the Mg lying on an inversion center resulting in two sets of crystallographically equivalent Mg–N bond distances of 2.075(3) and 2.059(3) Å, in good agreement with the Mg–N bond lengths in related Mg porphyrin systems (2.077(8) Å).[26] Unlike **Fe(III)TFP(Cl)**, the Mg center sits within the N_4 plane with N–Mg–N bond angles of 90.45(12) and 89.55(12)°, indicating a close to ideal square planar geometry within the porphyrin cavity. The crystals have disordered THF solvent molecules residing above and below the N_4 plane that feature close (< ~2.2 Å) Mg–O contacts, highlighting a significant interaction. Therefore, the coordination environment at the Mg center is best described as a pseudo-octahedral geometry.

The synthesis of iron **TFP** was first reported by Yokota and Fujii[27] to explore the defining factors in the heterolytic versus homolytic bond cleavage of terminal oxidants but the compound was yet to be structurally characterized. We *found* that **Fe(III)TFP(Cl)** crystallizes in the $P\bar{1}$ space group as a two-part twin. Refinement of the structure revealed an asymmetric unit containing two crystallographically distinct **Fe(III)TFP(Cl)** molecules as well as dichloromethane and highly-disordered pentane solvent molecules. The Fe centers are five-coordinate with a chloride ligand occupying one of the axial sites, likely derived from the dichloromethane solvent mixtures used for the synthesis and isolation of the molecule. The coordination environment at the Fe centers is best described as basally distorted square pyramidal ($\tau_5 = 0.01$) with the Fe displaced out of the mean N_4 plane of the porphyrin by an average of 0.492 Å towards the apical chloride.[28] The average Fe–N distance of 2.0675(11) Å corresponds well to the average Fe–N distance in related five-coordinate Fe porphyrin systems (2.05(2) Å) reported in the Cambridge Structural Database.[26] The average Fe–Cl bond distance of 2.2069(8) Å is also in line with the average Fe–Cl distance of 2.23(5) Å found in other reported Fe porphyrin systems containing apical chloride ligands.

Excited State Properties. The absorption spectra of the **Mg(II)TFP** and the **Fe(III)TFP(Cl)** porphyrins are shown in Figure 4. Consistent with the four-state Gouterman model,[29] the absorption *profile* is dominated by the Soret and Q bands. The D_{4h} high symmetry of the metalated porphyrins lead to fewer Q bands as compared to that observed of freebase **TFP**, which has D_{2h} symmetry. The blue-shift of the Soret and Q bands of **Fe(III)TFP(Cl)** relative to **Mg(II)TFP** is consistent with previous observations of hypso/hyper spectra of metalloporphyrins.[30,31] The mono-hydroxychlorin exhibits a broadened Soret band and several absorption bands in the Q-band region, consistent with the dramatically lowered symmetry of the macrocyclic core.

As expected for a metalloporphyrin with a partially occupied d-orbital, **Fe(III)TFP(Cl)** exhibits no appreciable emission owing to fast non-radiative decay from the porphyrin π-aromatic chromophore via the d-orbital manifold. In the absence of this non-radiative pathway, **Mg(II)TFP** and **2H-TFChl-$^{\beta}$OH** are highly emissive (Fig. 4). Time resolved kinetics of the emission spectra, shown in Fig. 5, fit to mono-exponential decays. The lifetime of **Mg(II)TFP** is similar to **TFP** (τ_o = 8.97 ns and 12.2 ns for **Mg(II)TFP** and **TFP**, respectively). Notably, in a direct comparison of mono-hydroxychlorin and porphyrin, the lifetime of **2H-TFChl-$^{\beta}$OH** of 11.3 ns is similar to its **TFP** and **Mg(II)TFP** congeners and to a reported lifetime of a dihydroxychlorin.[32] Replacement of the exchangeable protons with deuterium results in lengthening the exited state lifetime. However, this observed deuterium isotope effect appears to be related largely to the exchange of the protons on the pyrrolic nitrogens as **TFP** also exhibits a comparable increase in lifetime upon deuterium exchange.

CONCLUDING REMARKS

Peripheral substituents on metalloporphyrins can modulate the physical and chemical properties of the ring system within the biological milieu. Hydrogen bonding peripheral substituents are *especially* prevalent to function as they may directly interact with nearby amino acid side chains. The vinyl groups of protohemes,[33–35] and the formyl group of heme *a* in cytochrome oxidase[36] are exemplary manifestations of such hydrogen bonding effects in

biology. For example, changes in the strength of the formyl-protein hydrogen bond upon changes in the oxidation state of heme *a* have been proposed to be a mechanism for proton pumping in cytochrome *c* oxidase.[36–39] The perturbation of the electronic properties of the porphyrin macrocycles is assisted by conjugation of the periphery group to the aromatic 18π-electron pathway of the macrocycle. The 18π-electron aromatic pathway may be maintained upon saturation of the porphyrin framework, as the saturation of one of its *β,β′*-pyrrolic double bonds engenders a chlorin, which is the most important compound of porphyrin saturation as the chlorin macrocycle is the functional chromophore of chlorophylls.[40] Whereas formyl groups of various chlorophyll species are known to affect the electronic properties of the macrocycle,[41,42] the most prevalent perturbation arises from conjugation of the peripheral group to the 18π-electron framework of the chlorin.[43,44] A more subtle issue arises as to whether the presence of a hydrogen bond moiety situated at a site remote to the 18π-electron affects the electronic properties of chlorin. In view of the chlorin as the light-harvesting chromophore of photosynthesis, a particularly intriguing issue is whether the excited state properties of the chlorin ring are maintained with the presence of the O–H oscillator remote to the chlorin's 18π-electron pathway. Noting that the hydroxychlorins are relatively rare species, we have shown that formation of mono-hydroxychlorin may be obtained from the high dilution Lindsey porphyrin forming reaction if the reaction is performed in dry solvent and within the environment of a glovebox. The advantage of this method is that it affords hydroxychlorin without the use of harsh reagents such as OsO_4. We find that the excited state properties of the mono-hydroxychlorin are similar to that of its parent porphyrin congener. Thus, excited state deactivation by vibronic coupling to the high energy O–H oscillator is circumvented with the hydroxyl group remote to the 18π-electron framework of the chlorin ring. These results reveal that strong H-bonding groups may be introduced on to the chlorin ring while maintaining the light gathering properties that lie at the heart of photosynthesis of the chlorin ring.

EXPERIMENTAL

General Considerations

Hexane, pentane, CH_2Cl_2, Na_2SO_4, NaCl, $MgBr_2{\bullet}OEt_2$, $NaHCO_3$, triethylamine, 2,4,6-trimethylpyridine and other chemicals *were* obtained from commercial suppliers at the highest purity available and used without further purification. For the parallel synthesis of porphyrin and mono-hydroxychlorin, it was important to purify $CHCl_3$. $CHCl_3$ (500 mL) containing 0.5-1.0% EtOH as a stabilizer was placed in a 1000 mL oven-dried round bottom flask with excess potassium carbonate and a stir bar. The flask was affixed to a reflux condenser, distillation glassware, and Strauss flask. $CHCl_3$ was stirred, refluxed, and distilled. Over the course of 2 h, $CHCl_3$ (~450 mL) was collected in the Strauss flask. For further purification, distilled $CHCl_3$ in a closed Strauss flask was frozen in a dewar containing liquid nitrogen, pumped under vacuum, and thawed three times to remove gaseous impurities including oxygen. The degassed and distilled chloroform was covered with aluminum foil and stored away from light and transferred into the glove box to conduct the condensation reaction affording porphyrinogen *in situ*. To remove trace amounts of water, the purified $CHCl_3$ (450 mL) was dried over activated molecular sieves (3 Å).

^{1}H, ^{19}F, ^{13}C, ^{1}H-^{1}H COSY NMR spectra were recorded at the Harvard University Department of Chemistry and Chemical Biology NMR facility on a JEOL ECZ400S and Agilent DD2 600/(DD2-600) spectrometers operating at 400 MHz and 600 MHz, respectively. Absorption spectra were taken with a 1.0 cm quartz cuvette on a Varian Cary 5000 Uv-vis spectrophotometer. EPR spectra were obtained on a Bruker EleXsys E-500 CW-EPR spectrometer equipped with a quartz dewar containing liquid nitrogen. The EPR sample was prepared by dissolving 22.5 mM **Fe(III)TFP(Cl)** in toluene. The spectrum was measured with microwave power 0.06325 mW, microwave frequency 9.65 GHz, modulation amplitude 1 Gauss, and averaged over 16 scans. Effective g-values were obtained from spectral simulation of S = 5/2 with rhombicity using Easyspin. Zero-field ^{57}Fe Mössbauer spectra were collected on **Fe(III)TFP(Cl)** (32 mg, 0.036 mmol), which was frozen in benzene by rapid freezing in liquid nitrogen. The spectrum was measured with a constant acceleration SI-5 spectrometer (SEE Co, Minneapolis, MN) at 90 K. Isomer shifts are quoted relative to Fe foil at room temperature. Data were analyzed and simulated with Igor Pro 6 software (WaveMetrics, Portland, OR) using *Lorentzian* fitting functions. Steady-state emission spectra were measured on a fluorimeter Nejc will give me the info ~~(Photon Technology International, PTI model QM4) coupled to a 150 W Xe arc lamp as an excitation light source~~. Mass spectrometry was performed at the Harvard Center for Mass Spectrometry.

Synthesis of porphyrins and mono-hydroxychlorin

17,18-dihyro-18-hydroxy-5,10,15,20-tetrakis-(4-fluoro,2,6-dimethylphenyl)porphyrin (2H-TFChl-$^{\beta}$OH). In a nitrogen filled glovebox, 4-fluoro-2,6-dimethylbenzaldehyde (0.380 g, 2.50 mmol) and then pyrrole (0.174 mL, 2.500 mmol) were added *dropwise* to the oven dried round bottom flask containing dried and degassed $CHCl_3$ (250 mL). BF_3•OEt_2 (0.330 mL, 0.825 mmol) was added dropwise to the same flask with a syringe over 1 min. The reaction mixture was stirred for 1 h to form the porphyrinogen. At the end of 1 h, the reaction mixture was brought out of the glove box and *p*-chloranil (0.461g, 1.875 mmol) was added. The resulting reaction mixture was attached to an open-air reflux condenser and heated to reflux for an additional 1 h to facilitate the chemical oxidation reaction. The crude solid was delivered upon rotary evaporation and re-dissolved in a minimal amount of CH_2Cl_2. Purification over multiple silica flash columns (hexanes/CH_2Cl_2 3:1→1:2) followed by three additional pipette columns packed and eluted with hexanes (~100 mL) and THF afforded **2H-TFChl-$^{\beta}$OH** as a purple solid (8 mg, ~3% isolated yield). ^{1}H NMR (400 MHz, CD_2Cl_2): δ_H (ppm) 8.46 (m, 2H), 8.26 (m, 2H), 8.16 (d, J = 4.0 Hz, 1H), 8.14 (d, J = 4.0 Hz, 1H), 7.09–7.22 (m, 8H), 6.06 (m, 1H), 4.11 (dd, J = 8 Hz and J = 4 Hz, 1H), 3.8 (d, J = 20 Hz, 1H), 2.26 (d, J = 4 Hz, 1H), 2.66 (s, 3H), 2.05 (s, 3H), 1.92 (s, 3H), 1.90 (s, 3H), 1.88 (s, 3H), 1.82 (s, 3H), 1.78 (s, 3H), 1.73 (s, 3H), –1.74 (s, 2H) . ^{19}F NMR (376 MHz, THF-d_8): δ_F(ppm) –115.71 (s, 1F), –116.33 (s, 1F), –116.44 (s, 1F), –116.44 (s, 1F). ^{13}C NMR δ_c (ppm) 163.87, 163.34, 163.04, 161.73, 153.07, 152.39, 142.68, 141.59, 141.10, 140.69, 139.70, 139.53, 137.01, 136.80, 136.70, 136.04, 135.19, 134.66, 131.82, 131.46, 127.39, 127.00, 123.45, 122.76, 119.52, 118.64, 114.61, 114.47, 114.41, 114.34, 114.27, 114.20, 114.06, 113.45, 113.32, 109.40, 109.10, 73.80, 44.36, 36.53, 33.06, 31.93, 29.69, 24.74, 24.62, 23.07, 22.69, 21.54, 21.27, 21.21, 21.13, 20.70. ESI MS [(M

+ H)$^+$, M = $C_{52}H_{44}F_4N_4$] (m/z): calcd (817.3524), obsd (817.3534). λ_{abs} (CH_2Cl_2): 417, 516, 541, 591, 646 nm. λ_{em} = 654 nm (CH_2Cl_2, λ_{exc} ~~590~~ 415 nm). IR N–H 3351 cm^{-1}, O–H broad 3345–3352 cm^{-1}.

5,10,15,20-*Tetrakis*-(4-fluoro-2,6-dimethylphenyl)porphyrinatomagnesium(II)(Mg(II)TFP). By following reported procedure,[23] **TFP** (33 mg, 0.041 mmol) was dissolved in CH_2Cl_2 (2 mL) in a round-bottom flask with a stir bar. Triethylamine (0.111 mL, 0.796 mmol) was added dropwise through a syringe followed by addition of $MgBr_2$•OEt_2 (103 mg, 0.399 mmol). After 2 h, to prevent the reagents from drying, additional CH_2Cl_2 (4 mL), triethylamine (0.111 mL, 0.796 mmol), and $MgBr_2$•OEt_2 (103 mg, 0.399 mmol) were added. The resulting solution was heated at 41 °C for 48 h. The reaction was monitored by an aluminum TLC plate (2:1 Hexane/CH_2Cl_2). Upon disappearance of **TFP** on the TLC, the crude reaction mixture was dried on a rotary evaporator and treated with CH_2Cl_2 (~50 mL) and $NaHCO_3$. The organic phase was separated, treated with brine, and dried over Na_2SO_4. The crude reaction mixture was filtered, and the filtrate was concentrated to dryness, affording purple solid. The solid was introduced onto a neutral aluminum oxide flash column chromatography, packed with 1:1 Hexane/CH_2Cl_2 and eluted with 100% CH_2Cl_2. The eluted solution was concentrated to dryness affording magnesium porphyrin as a purple powder (27 mg, 80% isolated yield). ^{1}H NMR (400 MHz, CD_2Cl_2): δ_H (ppm) 8.56 (s, 8H), 7.15 (d, J = 8.0 Hz, 8H), 1.82 (s, 24H). ^{13}C NMR δ_c (ppm, 400 MHz, THF-d_8) 148.75, 141.57, 139.19.35, 130.24, 117.28, 113.15, 112.94, 31.95, 29.72, 29.38, 25.44, 22.64, 21.34, 13.51. ^{19}F NMR (376 MHz, THF-d_8): δ_F (ppm) −117.16 (triplet due to ^{1}H–^{19}F coupling, J = 9.4 Hz, 4F). ESI-MS [(M + H)$^+$, M = $C_{52}H_{40}$ F_4 MgN_4] (m/z): calcd (820.3034), obsd (820.3026). λ_{abs} (toluene): 426, 564, 603 nm. λ_{em} (toluene, excited at ~~573~~ 425 nm): 621, 678 nm.

5,10,15,20-*Tetrakis*-(4-fluoro-2,6-dimethylphenyl)porphyrinatoiron(III)(Fe(III)TFP(Cl)). Metalation of **TFP** with Fe was conducted in a nitrogen filled glovebox by following a published procedure.[45] **TFP** (32 mg, 0.04 mmol) was added to dry and degassed THF (10 mL) in a nitrogen filled glovebox. 2,4,6-Trimethylpyridine (10 µL, 0.08 mmol) was added and stirred for 10 min. At the end of 10 min, $FeBr_2$ (35 mg, 0.16 mmol) was added to the same flask. The resulting reaction mixture was stirred overnight and monitored by silica TLC plate (100% CH_2Cl_2). After confirming the completion of the metalation reaction, the flask was brought out of the glovebox and washed with water containing 10% trifluoracetic acid (20 mL). CH_2Cl_2 (30 mL) was added to this mixture. The organic layer was washed with brine, dried over Na_2SO_4, filtered, and concentrated to dryness. The resulting crude product was purified with silica flash column chromatography (100% CH_2Cl_2→10:1 EtOAc:MeOH) to afford a dark brown solid (44.7 mg, 40.4% isolated yield). ^{19}F NMR (376 MHz, THF-d_8): δ_F (ppm) –113.89. ESI-MS [(M + H)$^+$, M = $C_{52}H_{40}$ F_4 FeN_4] (m/z): calcd (852.2533), obsd (852.2568). λ_{abs} (CH_2Cl_2): 294, 417, 506 nm.

Crystallography

Mg(II)TFP (10 mg) was dissolved in dry THF (5 mL) and filtered through a 0.45 µm pore size filter. The filtrate was crystallized from dry THF in a small scintillation vial inside a nitrogen filled glovebox. Dry hexanes (~ 10 mL, anti-solvent) was added to a larger scintillation vial. The small scintillation vial was placed into the larger vial, covered loosely with the *scintillation* vial cap, and placed in a freezer at –35°C for two weeks to furnish dark purple crystals. Single crystal X-ray data of [$C_{52}N_4H_{40}F_4Mg$]•2THF was collected at 100 K using Mo IµS X-ray source on a

Bruker D8 Venture diffractometer with Photon III-C14 detector and Oxford 800+ Cryosystem. All non-H atoms, including the disordered fragment, were located in difference-Fourier maps, and then refined anisotropically. The restraints on bond lengths and constraints of the atomic displacement parameters on each pair of disorder fragments (SADI/SAME/FLAT and EADP instructions of SHELXL-2018), as well as the restraints of the atomic displacement parameters (SIMU/RIGU instructions of SHELXL-2018) if necessary, were applied for the disorder refinement. The disorder solvent molecules could not be located in the Fourier map and were squeezed out by using PLATON/SQUEEZE. The crystal was in accordance with a twin law "1 0 0, 0 –1 0, 0 0 –1"; however, a stable twinning processing and refinement model was not achieved because of the weak diffraction pattern. In this case, data was treated as a single domain and "plane background" was *used* for data integration. Crystal data, data collection, and structure refinement details are included in Table S1. Bond distances and bond angles are shown in Table S2.

Fe(III)TFP(Cl) (10 mg) was dissolved in dry CH_2Cl_2 (5 mL) and filtered through a 0.45µm pore size filter. The filtrate was crystallized from dry CH_2Cl_2 in a small scintillation vial inside the nitrogen atmosphere glovebox. Dry pentane (~10 mL, anti-solvent) was added to a larger *scintillation* vial covering around half the vial. The small scintillation vial was placed into the larger vial, covered loosely with the scintillation vial cap, and placed in a freezer at –35°C for two weeks to furnish dark brown crystals. Single crystal X-ray diffraction analysis of $2[(C_{52}N_4H_{40}F_4)FeCl]\cdot 0.876CH_2Cl_2\cdot 0.748C_5H_{12}$ was performed on a single crystal coated with Paratone-N oil and mounted on glass fibers. An Oxford Cryostream was used to keep crystals frozen at 100 K during data collection. Data were collected at ChemMatCARS at the Advanced Photon Source at Argonne National Laboratory using synchrotron radiation (λ = 0.41328 Å) on a Huber three-circle diffractometer equipped with a Pilatus 1M(CdTe) detector. The crystal was found to be a two-component non-merohedric twin based upon the diffraction pattern. The program CELL_NOW[46] was used to determine the orientation matrices. Both components raw data were integrated down to 0.84 Å resolution using Bruker AXS SAINT software[47] and absorption corrections were made using TWINABS.[48] Space group assignments were determined by examination of systematic absences, E-statistics, and successive refinement of the structures. Structures were solved by intrinsic phasing using SHELXT[49] and refined by least squares method using SHELXL[50] operated in the OLEX2[51] interface. All non-H atoms, including the disorder fragments, were located in difference Fourier maps and then refined anisotropically. Outlier reflections were omitted from refinement when appropriate. Hydrogen atoms were placed in ideal positions and refined using a riding model for all structures. Restraints on bond lengths (SADI/SAME) and on atomic displacement parameters (SIMU/RIGU) on each pair of disordered fragments, if necessary, have been applied for the disorder refinement. Crystal data, data collection, and structure refinement details are included in Table S3. Bond distances and bond angles are shown in Table S4.

Spectroscopy

Time-resolved emission ~~spectra~~ kinetics were collected with a Hamamatsu C4334 Streak Scope camera placed perpendicular to the excitation path. Measurements were taken in CH_2Cl_2 in the presence of air. The samples were

excited with 560 nm (**Mg(II)TFP**) or 590 nm (**TFP**, **2H-TFChl-$^{\beta}$OH**) light generated using an OPerA Solo (Coherent) femtosecond optical parametric amplifier seeded with fundamental pulses (800 nm, ~50 fs, 1kHz) from a Ti:sapphire regenerative amplifier (Coherent Libra-HE). The laser power was recorded as approximately 50 μW. Measurements were made with the following streak camera settings: a slit width of 500, a grating of 100 g mm^{-1} blazed at 450 nm, and a ruling of 100. Time resolved emission spectra were the result of the integration of 10,000 exposures. After integration over wavelength, the emission decay curves were fit to a single mono-exponential decay function using Phyton 3.0.

ACKNOWLEDGEMENTS

DKD acknowledges Harvard University, Department of Chemistry and Chemical Biology for support of this research and thanks Professor Daniel Nocera for scientific discussions. We thank the support to the X-ray facility from the Major Research Instrumentation (MRI) Program of the National Science Foundation (NSF) under Award Numbers 2216066. Use of the Advanced Photon Source, an Office of Science User Facility operated for the U.S. Department of Energy (DOE) Office of Science by Argonne National Laboratory, was supported by the DOE under Contract No. DE-AC02-06CH11357. B.M.C. acknowledges support from the National Science Foundation Graduate Research Fellowship Program under Grant DGE-2140743 and the Herchel Smith Graduate Fellowship Program at Harvard University. We thank Rui Sun and Chang Cui for their help in obtaining the EPR spectra and simulation, and Jeewhan Oh for help in obtaining the Mössbauer spectrum of **Fe(III)TFP(Cl)**.

SUPPORTING INFORMATION

Materials and methods, details on the synthesis, compound characterization data from ^{1}H, ^{13}C, ^{19}F NMR, IR, EPR, absorption and *emission*, and high-resolution mass spectrometry measurements; additional crystallographic data and metrical parameters; time-resolved emission decay profiles. Metrical and supplementary crystallographic data for the solid-state structures are available from the Cambridge Crystallographic Data Centre under reference numbers CCDC 2280558 and CCDC 2280188 for **Fe(III)TFP(Cl)** and **Mg(II)TFP**, respectively. These data can be obtained free of charge via www.ccdc.cam.ac.uk/data_request/cif, or by emailing data_request@ccdc.cam.ac.uk, or by contacting The Cambridge Crystallographic Data Centre, 12 Union Road, Cambridge CB2 1EZ, UK; fax: +44 1223 336033.

REFERENCES

1. Taniguchi M, Lindsey JS. Synthetic chlorins, possible surrogates for chlorophylls, prepared by derivatization of porphyrins. *Chem. Rev.* 2017; **117**, 344–535.
2. Lindsey JS. Synthesis of meso-substituted porphyrins. In *The Porphyrin Handbook*; Kadish KM, Smith KM, Guilard R (eds), Academic Press: San Diego, CA, 2000, Vol. 1, pp 45– 118.
3. Fischer H, Pfeifer HJ. Oxydation von porphyrinen und chlorinen mit osmiumtetroxyd. *Liebigs Ann. Chem*. 1944; **556**: 131–152.
4. Fischer H, Eckoldt H. Überführung von porphyrinen in dioxy-chlorine durch einwirkung von osmiumtetroxyd *Liebigs Ann. Chem*. 1940; **544**: 138–162.
5. Dolphin D, Brückner C. 2,3-*vic*-Dihydroxy-*meso*-tetraphenylchlorins from the osmium tetroxide oxidation of *meso*-tetraphenylporphyrin. *Tet Lett*. 1995; **36**: 3295–3298.
6. MacAlpine JK, Boch R, Dolphin D. Evaluation of tetraphenyl-2,3-dihydroxychlorins as potential photosensitizers. *J. Porph. Phtalocyanines* 2002; **6**: 146–155.
7. Dolphin D, Brückner C. *β-β´*-Dihydroxylation of *meso*-tetraphenylchlorins and metallochlorins *Tet Lett*. 1995; **36**: 9425–9428.
8. Banerjee S, Zeller M, Brückner C. OsO_4-mediated dihydroxylation of *meso*-tetraphenylporphyrin N-oxide and transformation of the resulting diolchlorin N-oxide regioisomers. *J. Org. Chem*. 2010; **75**:1179–1187.
9. Chang CK, Sotiriou C. C-Hydroxy- and C-Methylchlorins. A convenient route to heme d and bonellin model compounds. *J. Org. Chem.* 1985; **50**: 4989–4991.
10. Samankumara LP, Zeller M, Krausec JA and Brückner C. Syntheses, structures, modification, and optical properties of meso-tetraaryl-2,3-dimethoxychlorin, and two isomeric meso-tetraaryl-2,3,12,13-tetrahydroxybacteriochlorins. *Org. Biomol. Chem*. 2010; **8**: 1951–1965.
11. Akhigbe J, Samankumara LP and Brückner C. The breaking and mending of porphyrins: Reductive coupling of secochlorin bisaldehydes. *Tet. Lett*. 2012; **53**: 3524–3526.
12. Bataille CJR, Donohoe TJ. Osmium-free direct syn-dihydroxylation of alkenes. *Chem. Soc. Rev.* 2011; **40**, 114–128.
13. Achard T, Bellemin-Laponnaz S. Recent advances on catalytic osmium-free olefin *syn*-dihydroxylation. *Eur. J. Org. Chem.* 2021; 877–896
14. Chou P, Kim L, Marzouk SM, Sun R, Hartnett AC, Dogutan DK, Zheng SH and Nocera DG. Synthesis, characterization, and hydrogen evolution activity of metallo-*meso*-(4-fluoro-2,6-dimethylphenyl)porphyrin derivatives. *ACS Omega*, 2022; **7**: 8988–8994.
15. Wagner RW, Lawrence DS, Lindsey JS. An improved synthesis of tetramesitylporphyrin. *Tet. Lett.* 1987; **27**: 3069–3070.
16. Habermann SM, Murphy KP. Energetics of hydrogen bonding in proteins: a model compound study. *Protein Sci.* 1996; **5**, 1229–1239.
17. Yu B, Pletka CC, Iwahara J. NMR Observation of intermolecular hydrogen bonds between protein tyrosine side-chain OH and DNA phosphate groups. *Phys. Chem. B* 2020; **124**, 1065–1070.

18. Myers JK, Pace CN. Hydrogen bonding stabilizes globular proteins. *Biophys. J.* 1996; **71**, 2033–2039.
19. Hasegawa M, Ohmagari H, Tanaka H, Machida K. Luminescence of lanthanide complexes: From fundamental to prospective approaches related to water- and molecular-stimuli, *J. Photochem. Photobiol. C: Photochem. Rev.* 2022; **50**, 100484.
20. Horrocks WDW Jr, Sudnick DR. Lanthanide ion probes of structure in biology. Laser-induced luminescence decay constants provide a direct measure of the number of metal-coordinated water molecules. *J. Am. Chem. Soc.* 1979; **101**, 334–340.
21. Xiao D, Prémont-Schwarz, Nibbering ETJ, Batista VS. Ultrafast vibrational frequency shifts induced by electronic excitations: Naphthols in low dielectric media. *J. Phys. Chem. A* 2012; **116**, 2775–2790.
22. Murchie EH, Lawson T. Chlorophyll fluorescence analysis: A guide to good practice and understanding some new applications. *J. Exp. Botany* 2013; **64**, 3983–3998.
23. Lindsey JS, Woodford JN. A Simple method for preparing magnesium porphyrins. *Inorg. Chem.* 1995; **34**: 1063–1069.
24. Johnson EJ, Kleinlein C, Musgrave RA, Betley TA. Diiron oxo reactivity in a weak-field environment. *Chem. Sci.* 2019; **10**: 6304–6310.
25. Golbeck JH, van der Est A. Electron paramagnetic resonance spectroscopy In *Molecular Biophysics for the Life Sciences*, Allewell N, Nahri LO, Raymond I (eds), 2013, pp 175–213.
26. Groom CR, Bruno IJ, Lightfoot MP, Ward SC. The Cambridge structural database. *Acta. Cryst.* 2016; **B72**, 171– 179.
27. Yokota S, Fujii H. Critical factors in determining the heterolytic versus homolytic bond cleavage of terminal oxidants by iron(III) porphyrin complexes. *J. Am. Chem. Soc*. 2018; **140**, 5127–5137.
28. Addison AW, Rao TN, Reedijk J, Van Rijn J, Verschoor GC. Synthesis, structure, and spectroscopic properties of copper(II) compounds containing nitrogen–sulphur donor ligands; the crystal and molecular structure of aqua[1,7-bis(*N*-methylbenzimidazol-2′-yl)-2,6-dithiaheptane]copper(II) perchlorate. *J. Chem. Soc. Dalton Trans.* 1984; 1349–1356.
29. Gouterman M, Snyder LC, Wagnière GH. Spectra of porphyrins. Part II. Four orbital model. *J. Mol. Spectrosc.* 1963; **11**, 108–127.
30. Suslick KS, Watson RA. The photochemistry of chromium, manganese, and iron porphyrin complexes. *New J. Chem.* 1992; **16**, 633–642.
31. Marsh DF, Mink LM. Microscale synthesis and electronic absorption spectroscopy of tetraphenylporphyrin H_2(TPP) and metalloporphyrins Zn^{II}(TPP) and Ni^{II}(TPP). *J. Chem. Ed.* 1996; **73**, 1188–1190.
32. Al-Omari S. Photophysical properties and localization of chlorins substituted with methoxy groups, hydroxyl groups and alkyl chains in liposome-like cellular membrane. *Biomed. Mater*. 2007; **2**: 107–115.
33. Melin F, Hellwig P. Redox properties of the membrane proteins from the respiratory chain. *Chem. Rev.* 2020; **120**: 10244–10297.
34. Mie Y, Yamada C, Hareau GPJ, Neya S, Uno T, Funasaki N, Nishiyama K, Taniguchi I. Functional evaluation of heme vinyl groups in myoglobin with symmetric protoheme isomers. *Biochemistry* 2004; **43**: 13149–13155.

35. Kalsbeck WA, Robertson DE, Pandey RK, Smith KM, Dutton PL, Bocian DF. Structural and electronic properties of the heme cofactors in a multi-heme synthetic cytochrome. *Biochemistry* 1996; **35**: 3429–3438.
36. Ward B, Callahan, Young R, Babcock GT, Chang CK. Red shifts in the optical spectra of porphyrin Schiff bases upon protonation. *J. Am. Chem. Soc.* 1983; **105**: 636–638.
37. Capitanio G, Palese LL, Papa F, Papa S. Allosteric cooperativity in proton energy conversion in A1-type cytochrome *c* oxidase. *J. Mol. Biol.* 2020; **432**: 534–551.
38. Wikström M, Krab K, Sharma V. Oxygen activation and energy conservation by cytochrome *c* oxidase. *Chem. Rev.* 2018; **118**: 2469−2490.
39. Yoshikawa S, Shimada A. Reaction mechanism of cytochrome *c* oxidase. *Chem. Rev.* 2015; **115**: 1936–1989.
40. Taniguchi M, Lindsey JS. Synthetic chlorins, possible surrogates for chlorophylls, prepared by derivatization of porphyrins. *Chem. Rev.* 2017; **117**: 344–535.
41. Schliep M, Cavigliasso G, Quinnell RG, Stranger R, Larkum AWD. Formyl group modification of chlorophyll *a*: A major evolutionary mechanism in oxygenic photosynthesis. *Plant Cell Environ.* 2013; **36**: 521–527.
42. Chen M. Chlorophyll modifications and their spectral extension in oxygenic photosynthesis. *Annu. Rev. Biochem.* 2014; **83**: 317–340.
43. Effects of substituents on synthetic analogs of chlorophylls. Part 1: Synthesis, vibrational properties and excited-state decay characteristics. Hooi Ling Kee 1, Christine Kirmaier, Qun Tang, James R Diers, Chinnasamy Muthiah, Masahiko Taniguchi, Joydev K Laha, Marcin Ptaszek, Jonathan S Lindsey, David F Bocian, Dewey Holten. *Photochem Photobiol*. 2007; **83**:1110–11124.
44. Faries KM, Diers JR, Springer JW, Yang E, Ptaszek M, Lahaye D, Krayer M, Taniguchi M, Kirmaier C, Lindsey JS, Bocian DF, Holten D. Photophysical properties and electronic structure of chlorin-imides: Bridging the gap between chlorins and bacteriochlorins. *J. Phys. Chem. B* 2015; **119**: 7503−7515.
45. Amanullah S, Das KP, Samanta S and Dey A. Tuning the thermodynamic onset potential of electrocatalytic O_2 reduction reaction by synthetic iron–porphyrin complexes. *Chem. Comm*. 2015; **51**, 10010–100138.
46. Sheldrick GM. CELL NOW V2008/2; Bruker AXS Inc; Bruker AXS Inc, 2008.
47. B.A.X.S. Inc., SAINT and APEX 2 Software for CCD Diffractometers (Bruker Analytical X-ray Systems, Inc., 2000), Bruker Analytical X-ray Systems, Inc.
48. Sheldrick GM. SADABS (Bruker Analytical X-ray Systems, Inc., 2014), Bruker Analytical X-ray Systems, Inc.
49. Sheldrick GM. SHELXT- integrated space-group and crystal-structure determination. *Acta Cryst.* 2015; **A71**, 3–8.
50. Sheldrick GM. SHELXL (University of Göttingen, Germany, 2014), University of Göttingen, Germany.
51. Dolomanov OV, Bourhis LJ, Gildea RJ, Howard JAK, Puschmann H. OLEX2: A complete structure solution, refinement and analysis program. *J. Appl. Cryst.* 2009; **42**, 339–341.

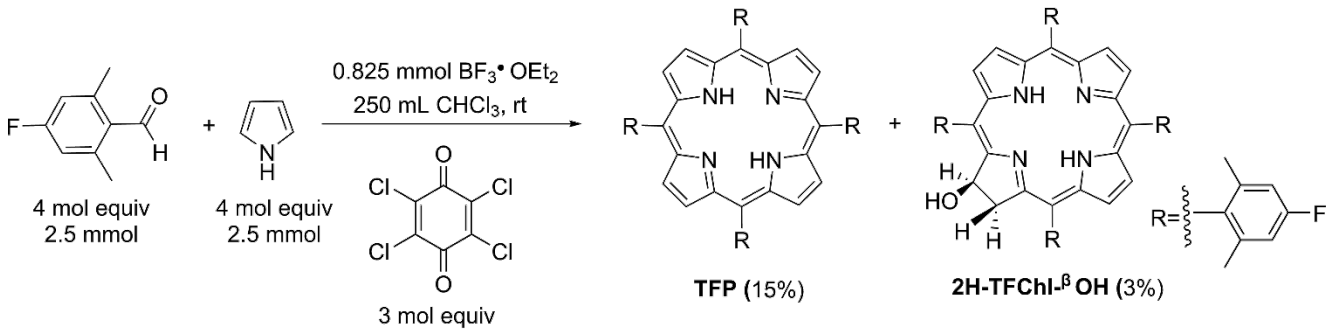

Fig. 1. Synthesis of *tetra*-4-fluoro-2,6-dimethylphenyl porphyrin and mono-hydroxychlorin complexes.

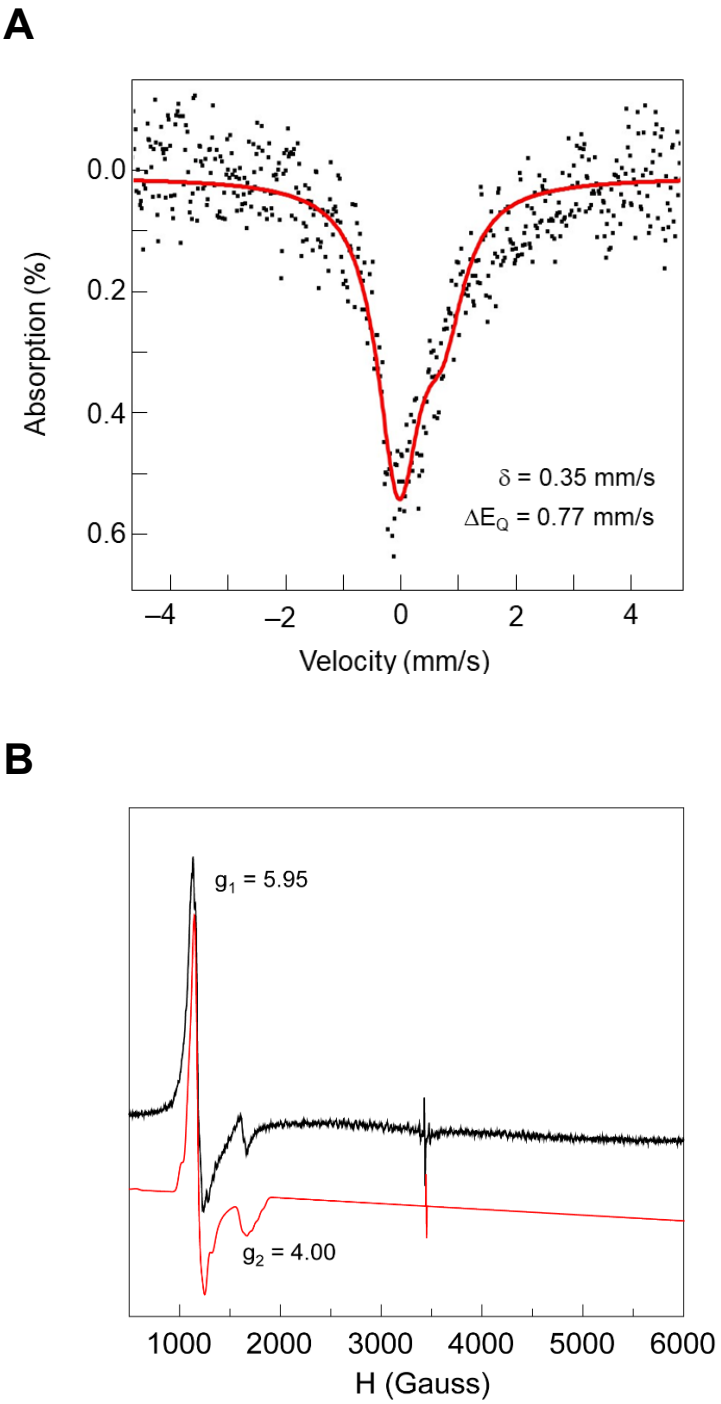

Fig. 2. Spectroscopic characterization of **Fe(III)TFP(Cl)**. (**A**) Mössbauer spectrum of **Fe(III)TFP(Cl)** in a frozen benzene matrix at 90 K. (**B**) EPR spectrum of **Fe(III)TFP(Cl)** (black trace) in toluene at 77 K and the simulated spectrum (red line).

A

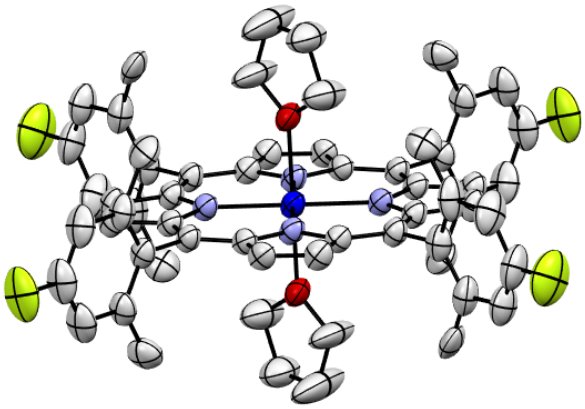

B

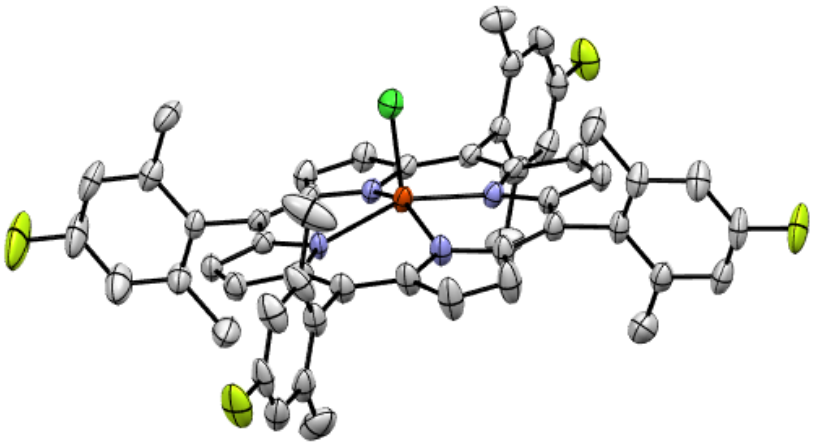

Fig.3. Crystal structures of (**A**) **Mg(II)TFP** and (**B**) **Fe(III)TFP(Cl)**. **Mg(II)TFP** color scheme: Mg (dark blue), N (light purple), O (red), F (yellow), C (grey) and Hydrogens are omitted for clarity. **Fe(III)TFP(Cl)** color scheme**:** Fe (red), N (purple), Cl (bright green), F (yellow), C (light grey).Hydrogens are omitted for clarity. (white).

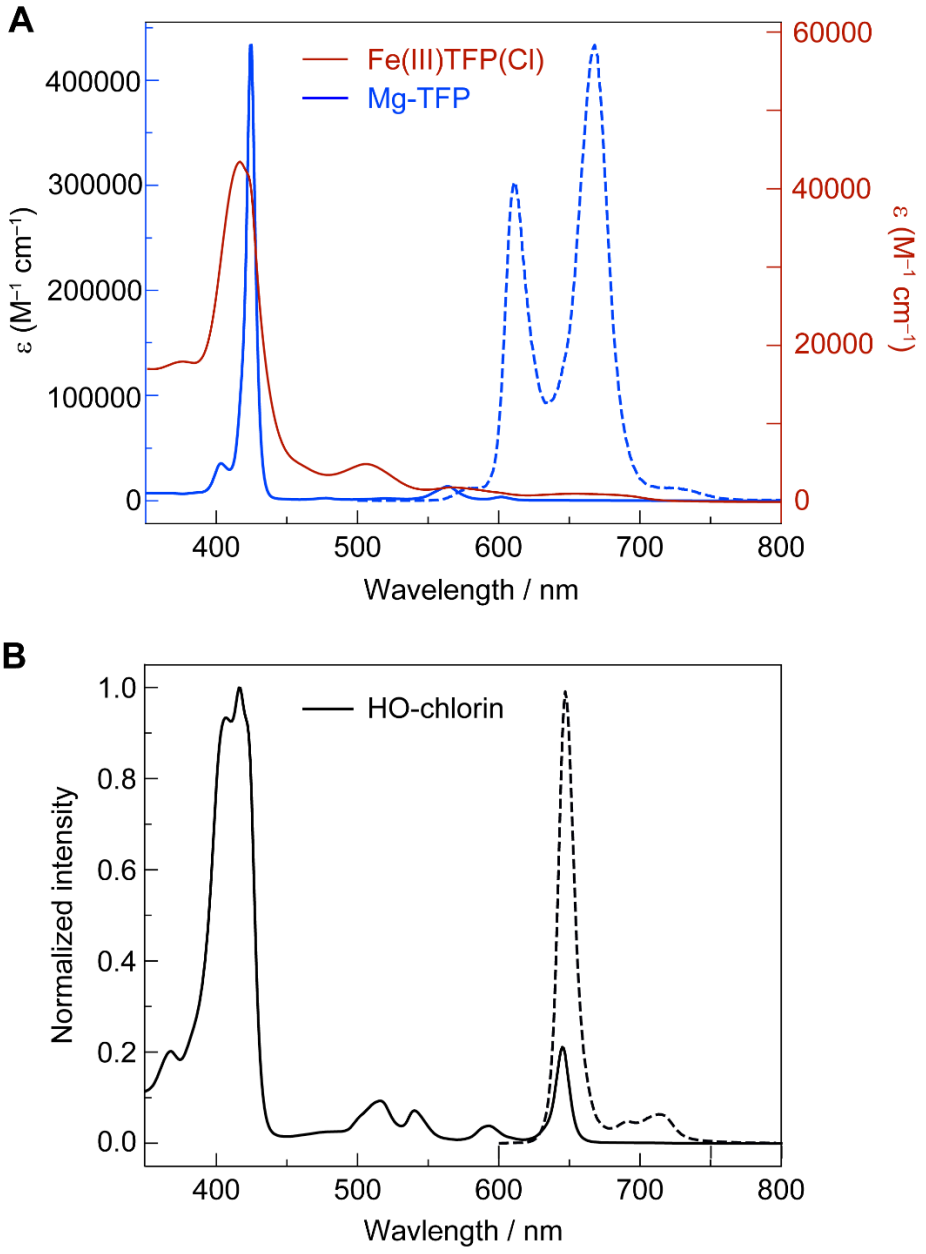

Fig. 4. Electronic absorption spectra of (**A**) **Mg(II)TFP** (blue) and **Fe(III)TFP(Cl)** (red) porphyrins and (**B**) **2H-TFChl-$^{\beta}$OH**. The normalized emission spectra are shown by the dashed lines. **Mg(II)TFP**, toluene, λ_{exc} 425 nm and **2H-TFChl-$^{\beta}$OH,** CH_2Cl_2, λ_{exc} 415 nm.

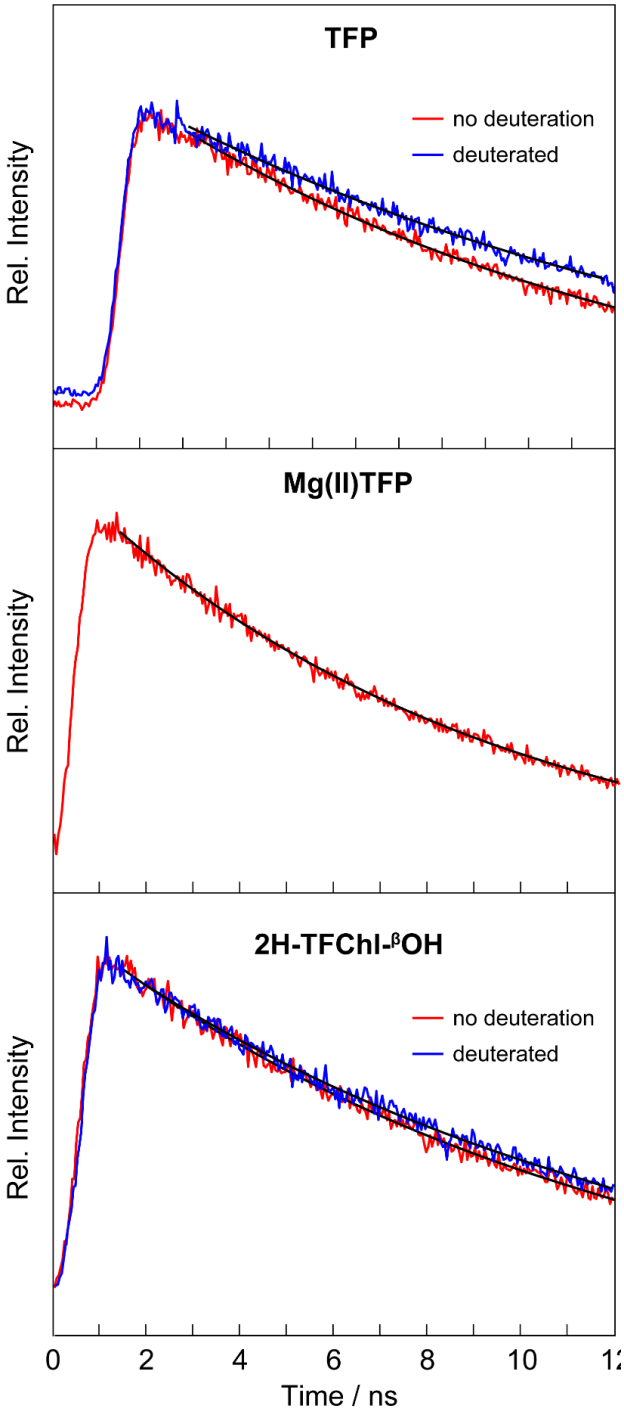

Fig. 5. Time-resolved emission decay traces of **TFP**, **Mg(II)TFP** and **2H-TFChl-$^{\beta}$OH**. For **TFP** and **2H-TFChl-$^{\beta}$OH**, the decay traces were also collected for deuterium exchanged compounds. The black lines correspond to the mono-exponential fits with lifetimes of 12.2 ns and 15.0 ns for non-deuterated and deuterated **TFP**, 8.97 ns for **Mg(II)TFP**, and 11.3 ns and 12.3 ns non-deuterated and deuterated **2H-TFChl-$^{\beta}$OH/D**, respectively. The lifetimes are plotted on a linear scale.